


Cite this: *RSC Adv.*, 2025, 15, 47203

Novel quinolinyl-thiazole hybrid candidates bearing *N*-methyl piperazine as potential anti-breast cancer agents: synthesis, biological evaluation and computational studies

Archana B. Dhongade,^a Umang Shah,^b Bhausaheb N. Patil,^c Rahul A. Shinde,^d Ruma Sarkar,^e Adrija Mukherjee,^e Suraj N. Mali,^f Vishnu A. Adole^{*,a} and Thansing B. Pawar^{*,a}

Breast cancer remains one of the most pressing global health concerns, emphasizing the urgent need for novel and effective therapeutic strategies. In this context, a new series of quinolinyl-thiazole derivatives incorporating an *N*-methyl piperazine moiety (**6a–6h**) was rationally designed, synthesized, and thoroughly characterized using FT-IR, ¹H NMR, ¹³C NMR, and mass spectral methods. The anti-breast cancer potential of these compounds was assessed against the triple-negative breast cancer cell line MDA-MB-231, exhibiting IC₅₀ values ranging from 1.415 ± 0.16 to 2.898 ± 0.27 μM, thus highlighting their anti-breast cancer potential. Within the series, compound **6a** showed the highest potency with the lowest IC₅₀ value, whereas **6f** displayed the weakest activity. Molecular docking of quinolinyl-thiazole derivatives (**6a**, **6f**, **6g** and **6h**) against epidermal growth factor receptor tyrosine kinase revealed binding affinities correlating with their *in vitro* cytotoxicity on MDA-MB-231 cells, with **6a** showing the strongest activity (IC₅₀ = 1.415 ± 0.16 μM; docking score = −10.0 kcal mol^{−1}) via key hydrogen bonds, electrostatic contacts, and hydrophobic interactions. Furthermore, *in silico* ADME evaluation and drug-likeness analysis indicated that all synthesized derivatives possessed favorable pharmacokinetic properties. Density functional theory analysis of the most potent compound (**6a**) offered valuable insights into its structural characteristics, electronic distribution, and chemical reactivity via optimized geometry, frontier molecular orbital and molecular electrostatic potential surface studies. The results suggested that the synthesized compounds are promising candidates for further investigation.

Received 26th August 2025
Accepted 10th October 2025

DOI: 10.1039/d5ra06350g

rsc.li/rsc-advances

1. Introduction

Cancer is one of the most pressing global health issues, with breast cancer being the most commonly diagnosed malignancy and the leading cause of cancer-related deaths among women globally.^{1–3} Challenges such as drug resistance, systemic toxicity, and tumor heterogeneity continue to impede effective breast cancer treatment.^{4–6} As a result, the discovery of new bioactive compounds with superior potency, selectivity, and pharmacokinetic features is important.^{7–9} Heterocyclic compounds have generated significant interest in anticancer research due to their structural versatility and biological significance.^{10,11} Thiazole and quinoline scaffolds, in particular, have emerged as key pharmacophores in the development of strong anticancer drugs.^{12,13} Thiazole, a five-membered heterocycle containing both sulfur and nitrogen atoms, is a core unit in various FDA-approved drugs and bioactive molecules.^{14,15} Thiazole derivatives have exhibited promising activity against cancer cells through diverse mechanisms, including DNA intercalation, tubulin polymerization inhibition, apoptosis induction, and kinase modulation.^{16–20}

^aResearch Centre in Chemistry, Mahatma Gandhi Vidyamandir's Loknete Vyankatrao Hiray Arts, Science and Commerce College (Affiliated to Savitribai Phule Pune University, Pune), Panchavati, Nashik 422003, Pune, India. E-mail: archanadhongde16@gmail.com; vishnuadole86@gmail.com; tbpawar03@gmail.com

^bRamanbhai Patel College of Pharmacy, Charotar University of Science and Technology (CHARUSAT), CHARUSAT campus, Changa 388421, India. E-mail: umangshah.ph@gmail.com

^cCSIR National Chemical Laboratory, Pune-411008, India. E-mail: manishpatil241187@gmail.com

^dDepartment of Chemistry, Mahatma Gandhi Vidyamandir's Maharaja Sayajirao Gaikwad Arts, Science and Commerce College (Affiliated to Savitribai Phule Pune University, Pune), Malegaon, Nashik 423105, India. E-mail: rahulshinde843@gmail.com

^eB. D. Patel Institute of Paramedical Sciences, Charotar University of Science and Technology, CHARUSAT Campus, Changa 388421, Gujarat, India. E-mail: rumasarkar.cips@charusat.ac.in; adituli98mukherjee@gmail.com

^fSchool of Pharmacy, DY Patil University, Navi Mumbai-400706, Maharashtra, India. E-mail: mali.suraj1695@gmail.com



Several clinically useful anticancer drugs, such as dasatinib and tiazofurin, feature the thiazole nucleus, underlining its therapeutic relevance.^{12,21,22} On the other hand, quinoline, a fused aromatic nitrogen-containing heterocycle, is another scaffold widely explored in medicinal chemistry.^{23–25} Its derivatives are known for diverse pharmacological activities, particularly as anticancer, antimalarial, and antimicrobial agents.^{26–28}

Hybridization of pharmacophores represent a strategic approach in modern drug design, wherein two or more bioactive moieties are integrated into a single molecular entity to enhance biological activity and improve target specificity.^{29,30} The fusion of thiazole and quinoline into a single framework, therefore, holds significant promise for generating potent anticancer agents.^{31,32} In last two decades, medicinal chemists have incorporated piperazine and its derivatives as functional components in drug design due to their favorable pharmacological attributes.^{33–35} It enhances drug–receptor interactions, and is a common motif in drugs such as imatinib and flunarizine.^{36,37} Fig. 1 represents bioactive compounds incorporating quinoline, thiazole, and piperazine scaffolds, known for their diverse pharmacological activities.

In silico molecular modelling techniques such as molecular docking, absorption, distribution, metabolism, and excretion (ADME) profiling, and density functional theory (DFT) studies have become indispensable tools in modern drug development.^{38–40} It has been previously reported that targeting the epidermal growth factor receptor (EGFR) is an effective strategy for investigating drug–receptor interactions, particularly in the context of developing and evaluating compounds with potential anti-breast cancer activity.^{41–44} Molecular docking provides insights into the binding affinity and interaction profile between synthesized compounds and EGFR which is frequently overexpressed in breast cancer.^{45,46} Triple-negative breast cancer (TNBC) is an aggressive type of breast cancer lacking estrogen receptor (ER), progesterone receptor (PR), and human epidermal growth factor receptor 2 (HER2), and some TNBC tumors have high epidermal growth factor receptor (EGFR) levels, which drive tumor growth and poor outcomes, making EGFR a useful target for developing new therapies.^{47–51} In this context, the present study was undertaken with the objective of designing and synthesizing novel quinoline-thiazole hybrid derivatives bearing *N*-methyl piperazine as potential antibreast cancer candidates. A concise synthetic strategy was adopted,

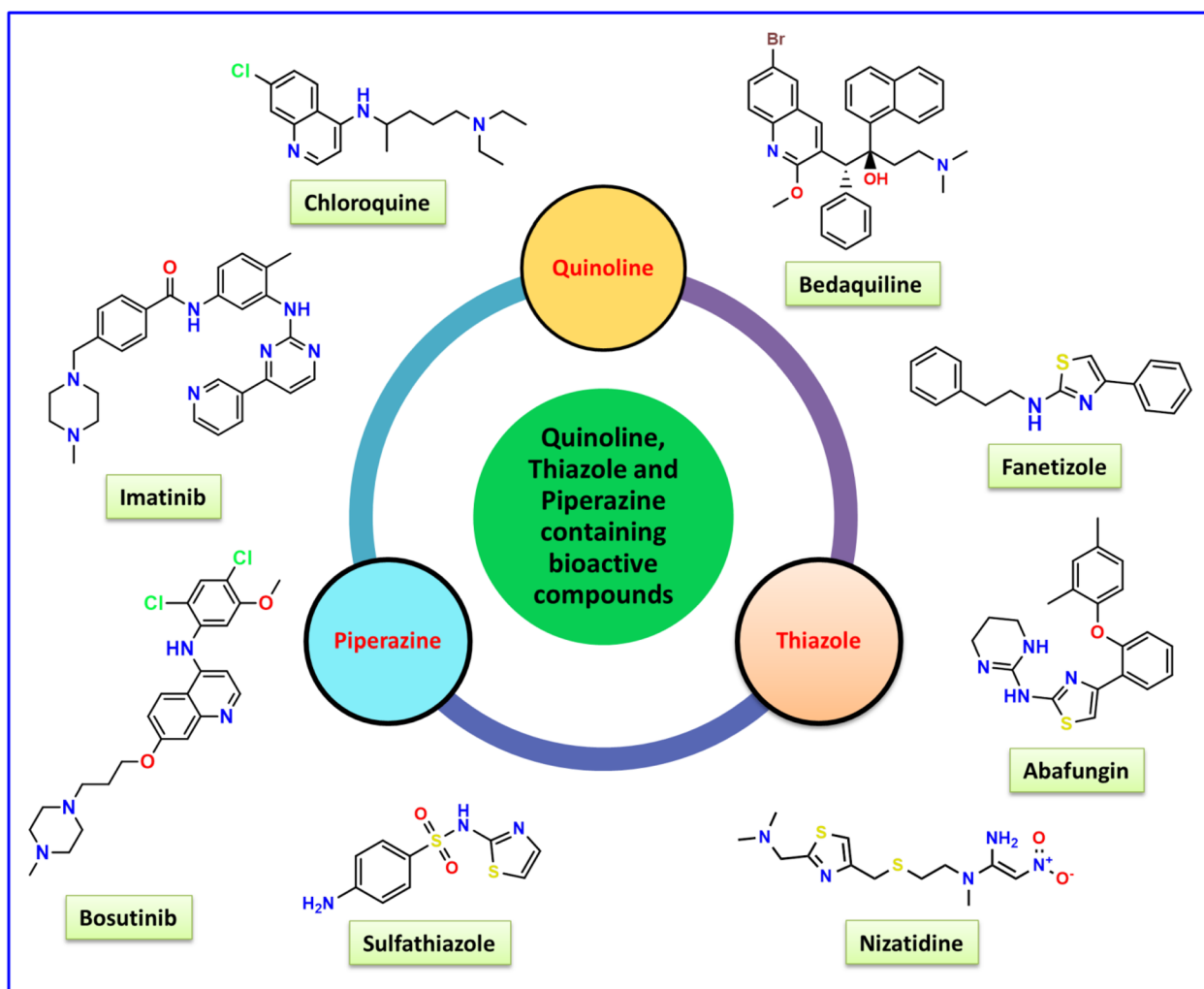


Fig. 1 Bioactive compounds featuring quinoline, thiazole and piperazine structures.



enabling the construction of the hybrid framework in good yields with structural confirmation through spectroscopic techniques including FT-IR, ^1H and ^{13}C NMR, and mass spectral techniques. The synthesized compounds were subjected to Anti-Breast cancer activity against triple negative breast cancer cell line (MDA-MB-231) using MTT assay to evaluate their cytotoxic efficacy. Furthermore, molecular docking studies were carried out to predict the binding interactions of the most active compounds. ADME properties were also computed to assess their drug-likeness and pharmacokinetic suitability. The novelty of this work lies in the rational design of a new class of quinoline-thiazole hybrids integrated with a *N*-methyl piperazine unit, aiming for enhanced cytotoxicity against breast cancer cells. This multi-faceted approach combining organic synthesis, biological evaluation, and molecular modelling offers a robust platform for the discovery of new anticancer agents.

2. Materials and methods

2.1. General remarks

All reagents and solvents were procured from commercial suppliers and used without further purification. Reaction progress was monitored by thin-layer chromatography (TLC) on silica gel plates using appropriate solvent systems, and spots were visualized under UV light. The melting points of the synthesized compounds were determined in open capillaries and are uncorrected. The purity of final compounds (**6a–6h**) was confirmed by TLC and characterized using FT-IR, ^1H NMR, ^{13}C NMR, and mass spectrometry.

2.2. Synthetic procedure

2.2.1. Step (i): synthesis of intermediate 2. To a stirred solution of *N*-acetylaniline (compound **1**) in dry dimethylformamide (DMF), phosphorus oxychloride (POCl_3) was added dropwise under cooling. The reaction mixture was then refluxed for 8 hours. The progress of the reaction was monitored using TLC. After completion, the reaction mixture was cooled to room temperature and poured onto crushed ice with continuous stirring. The resulting precipitate was filtered, washed with water, and purified by using isopropyl alcohol to obtain the intermediate 2-chloroquinoline-3-carbaldehyde (**2**) in good yield.

2.2.2. Step (ii): synthesis of intermediate 3. In a separate round-bottom flask, compound **2** was reacted with *N*-methylpiperazine (1.2 equivalents) in the presence of anhydrous potassium carbonate (K_2CO_3) as a base in dry DMF as the solvent. The mixture was heated at 110–120 °C for 5 hours with constant stirring. This step facilitates the nucleophilic substitution of the chloro group by the *N*-methylpiperazine unit. Upon reaction completion (monitored by TLC), the reaction mass was cooled, poured into ice-cold water, and extracted with ethyl acetate. The organic layer was washed with water and brine, dried over anhydrous sodium sulfate, and concentrated under reduced pressure. The residue was purified by using isopropyl alcohol to obtain the pure compound **3**.

2.2.3. Step (iii): synthesis of quinolyl-thiazole hybrids (6a–6h). Quinolyl-thiazole hybrids (**6a–6h**) were prepared as per previously published method with slight modification.⁵² A mixture of intermediate **3** (255.32 mg, 1.00 mmol) and thiosemicarbazide (**4**, 91 mg, 1.00 mmol) was placed in a 25 mL round-bottom flask containing PEG-400 (5 mL) and 10 mol% sulfamic acid (9.71 mg, 0.10 mmol). The mixture was stirred and heated at 80–90 °C for 60 minutes to allow initial condensation. Subsequently, the substituted phenacyl bromide derivative (**5a–5h**, 1.00 mmol) was added directly to the hot reaction mixture. Heating was continued at 80–90 °C for an additional 15 minutes until completion, monitored by TLC. The reaction mixture was cooled to room temperature and ice cold water (20–30 mL) was added with stirring, and the precipitate was filtered, washed with cold ethanol and dried at room temperature. The crude products were purified by recrystallization using ethanol to afford pure hybrid compounds **6a–6h** (Scheme 1).

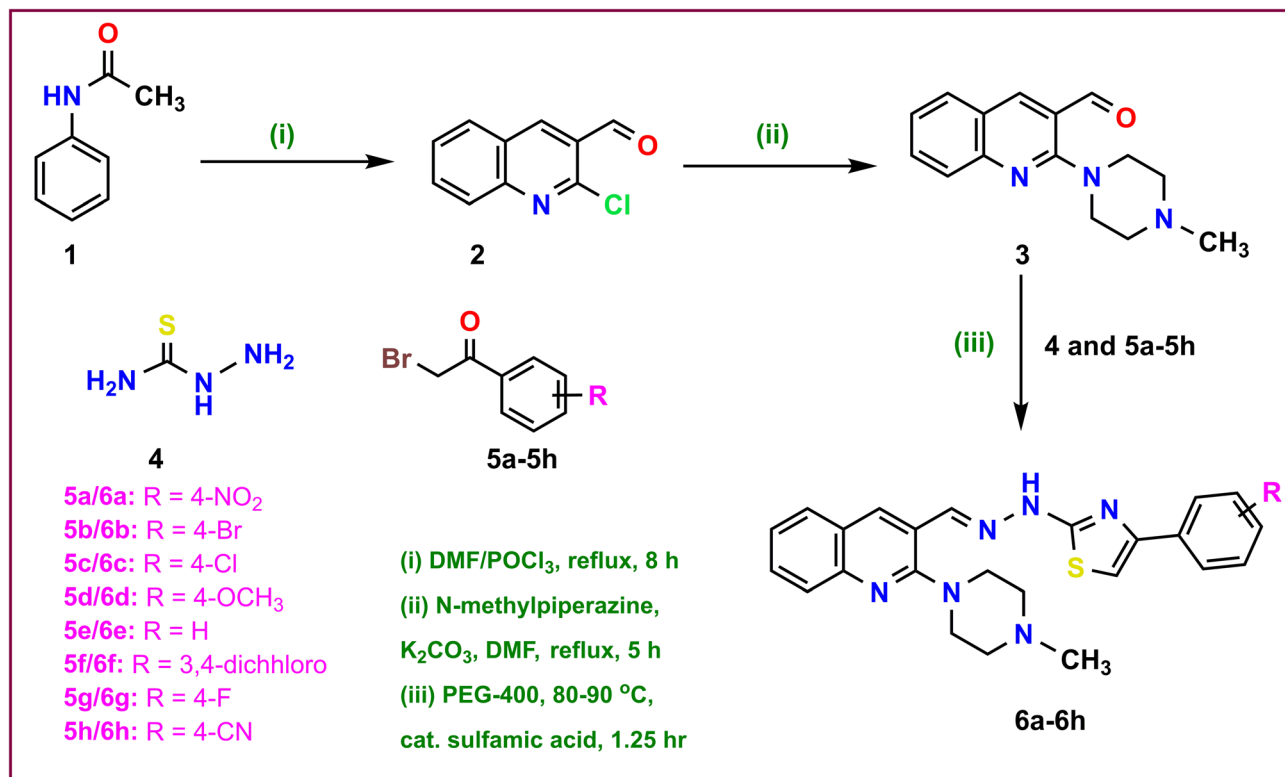
2.3. Spectral data

2.3.1. 2-(4-methylpiperazin-1-yl)quinoline-3-carbaldehyde (3). ^1H NMR (500 MHz, CDCl_3) δ 10.18 (s, 1H), 8.49 (s, 1H), 7.86–7.77 (m, 2H), 7.72–7.67 (m, 1H), 7.37 (t, $J = 7.5$ Hz, 1H), 3.59–3.50 (m, 4H), 2.70–2.61 (m, 4H), 2.39 (s, 3H); ^{13}C NMR (126 MHz, CDCl_3) δ 190.27, 159.05, 149.35, 142.28, 132.47, 129.27, 127.57, 124.62, 124.03, 122.11, 77.30, 77.04, 76.79, 55.00, 51.04, 46.18; MS for $\text{C}_{15}\text{H}_{17}\text{N}_3\text{O}$: $[\text{M} + \text{H}]^+$ calculated m/z : 256.14 and observed: 256.1448.

2.3.2. (E)-2-(2-((2-(4-methylpiperazin-1-yl)quinolin-3-yl)methylene)hydrazineyl)-4-(4-nitrophenyl)thiazole (6a). FT-IR (cm^{-1}): 3176, 3103, 2920, 2845, 1595, 1560, 1516, 1456, 1437, 1408, 1273, 1153, 1047, 1015, 984, 945, 847, 755, 686, 530; ^1H NMR (500 MHz, $\text{DMSO}-d_6$) δ : 12.47 (s, 1H), 8.59 (s, 1H), 8.30 (d, $J = 8.6$ Hz, 2H), 8.25 (s, 1H), 8.14 (d, $J = 8.6$ Hz, 2H), 8.05–8.00 (m, 1H), 7.82–7.78 (m, 2H), 7.72–7.68 (m, 1H), 7.51–7.47 (m, 1H), 3.33 (s, 8H), 2.88 (s, 3H); ^{13}C NMR (126 MHz, $\text{DMSO}-d_6$) δ : 168.12, 157.46, 148.45, 146.15, 146.01, 140.46, 138.25, 134.46, 130.24, 128.23, 127.07, 126.25, 125.14, 124.98, 124.04, 120.86, 108.78, 52.55, 47.33, 42.46; MS for $\text{C}_{24}\text{H}_{23}\text{N}_7\text{O}_2\text{S}$: $[\text{M} + \text{H}]^+$ calculated m/z : 474.17 and observed: 474.2784.

2.3.3. (E)-4-(4-bromophenyl)-2-(2-((2-(4-methylpiperazin-1-yl)quinolin-3-yl)methylene)hydrazineyl)thiazole (6b). FT-IR (cm^{-1}): 3365, 3169, 3048, 2982, 2899, 2843, 1607, 1482, 1433, 1353, 1283, 1240, 1158, 1047, 998, 948, 855, 786, 749, 686, 663, 542; ^1H NMR (500 MHz, $\text{DMSO}-d_6$) δ : 12.37 (s, 1H), 8.58 (s, 1H), 8.23 (s, 1H), 8.05–7.99 (m, 1H), 7.83 (d, $J = 8.4$ Hz, 2H), 7.81–7.79 (m, 1H), 7.72–7.68 (m, 1H), 7.62 (d, $J = 8.4$ Hz, 2H), 7.50–7.46 (m, 2H), 3.33 (s, 8H), 2.89 (s, 3H); ^{13}C NMR (126 MHz, $\text{DMSO}-d_6$) δ : 167.81, 157.43, 149.29, 145.95, 137.88, 134.37, 133.68, 131.48, 130.19, 128.20, 127.44, 127.06, 125.13, 125.00, 120.93, 120.51, 104.79, 52.50, 47.26, 42.39; MS for $\text{C}_{24}\text{H}_{23}\text{BrN}_6\text{S}$: $[\text{M} + \text{H}]^+$ calculated m/z : 507.09 and observed: 507.2186.

2.3.4. (E)-4-(4-chlorophenyl)-2-(2-((2-(4-methylpiperazin-1-yl)quinolin-3-yl)methylene)hydrazineyl)thiazole (6c). FT-IR (cm^{-1}): 3364, 3170, 3052, 2983, 2843, 1644, 1608, 1484, 1355, 1283, 1241, 1159, 1088, 1048, 948, 916, 855, 787, 667, 519; ^1H NMR (500 MHz, $\text{DMSO}-d_6$) δ : 12.37 (s, 1H), 8.57 (s, 1H), 8.24 (s,



Scheme 1 Synthetic pathway for the preparation of novel quinolinyl-thiazole hybrid candidates (**6a–6h**) bearing *N*-methylpiperazine via three-step synthesis involving quinoline formation, piperazine substitution, and final condensation and cyclization with thiosemicarbazide and phenacyl bromide derivatives.

1H), 8.04–8.00 (m, J = 8.0 Hz, 1H), 7.90 (d, J = 6.8 Hz, 2H), 7.81–7.78 (m, J = 8.3 Hz, 1H), 7.71–7.68 (m, J = 7.4 Hz, 1H), 7.50–7.46 (m, J = 9.3 Hz, 4H), 3.35 (s, 8H), 2.87 (s, 3H); ¹³C NMR (126 MHz, DMSO-*d*₆) δ : 168.39, 158.07, 149.80, 146.54, 138.46, 134.91, 133.92, 132.48, 130.75, 129.14, 128.77, 127.70, 127.63, 125.68, 125.56, 121.52, 105.26, 53.16, 47.97, 43.12; MS for C₂₄H₂₃ClN₆S: [M + H]⁺ calculated m/z : 463.14 and observed: 463.2554.

2.3.5. (E)-4-(4-methoxyphenyl)-2-(2-((2-(4-methylpiperazin-1-yl)quinolin-3-yl)methylene)hydrazineyl)thiazole (6d). FT-IR (cm⁻¹): 3358, 3164, 3044, 2977, 2839, 1648, 1608, 1552, 1489, 1355, 1168, 1053, 989, 833, 788, 695, 527; ¹H NMR (500 MHz, DMSO-*d*₆) δ : 12.31 (s, 1H), 8.58 (s, 1H), 8.22 (s, 1H), 8.05–8.01 (m, 1H), 7.86–7.77 (m, 3H), 7.74–7.68 (m, 1H), 7.51–7.46 (m, 1H), 7.23 (s, 1H), 6.98 (d, J = 8.6 Hz, 2H), 3.80 (s, 3H), 3.33 (s, 8H), 2.93 (s, 3H); ¹³C NMR (126 MHz, DMSO-*d*₆) δ : 167.53, 158.75, 157.34, 150.33, 145.90, 137.49, 134.27, 130.16, 128.19, 127.37, 127.07, 126.76, 125.16, 125.05, 121.01, 113.91, 101.73, 55.06, 52.38, 47.05, 42.17; MS for C₂₅H₂₆N₆OS: [M + H]⁺ calculated: 459.19 and observed: 459.3092.

2.3.6. (E)-2-(2-((2-(4-methylpiperazin-1-yl)quinolin-3-yl)methylene)hydrazineyl)-4-phenylthiazole (6e). FT-IR (cm⁻¹): 3346, 3148, 3058, 2958, 2845, 1638, 1604, 1553, 1487, 1356, 1281, 1161, 1050, 990, 849, 779, 695, 539; ¹H NMR (500 MHz, DMSO-*d*₆) δ : 12.35 (s, 1H), 8.58 (s, 1H), 8.23 (s, 1H), 8.05–8.01 (m, J = 8.1 Hz, 1H), 7.88 (d, J = 7.8 Hz, 2H), 7.82–7.79 (m, J = 8.4 Hz, 1H), 7.72–7.68 (m, J = 7.6 Hz, 1H), 7.49 (t, J = 7.5 Hz, 1H), 7.45–7.39 (m, J = 13.0, 5.2 Hz, 3H), 7.34–7.30 (m, J = 7.3 Hz, 1H), 3.33 (s, 8H), 2.93 (s, 3H); 157.36, 150.49, 145.92, 137.45,

134.46, 133.48, 129.56, 128.20, 127.57, 127.02, 125.42, 125.04, 120.98, 108.89, 67.65, 52.38, 42.09, 42.17; MS for C₂₄H₂₄N₆S: [M + H]⁺ calculated m/z : 429.18 and observed: 429.2868.

2.3.7. (E)-4-(3,4-dichlorophenyl)-2-(2-((2-(4-methylpiperazin-1-yl)quinolin-3-yl)methylene)hydrazineyl)thiazole (6f). FT-IR (cm⁻¹): 3161, 3100, 2980, 2921, 2849, 1595, 1565, 1489, 1453, 1410, 1385, 1358, 1295, 1133, 1054, 986, 936, 876, 787, 679, 557; ¹H NMR (500 MHz, DMSO-*d*₆) δ : 12.40 (s, 1H), 8.58 (s, 1H), 8.23 (s, 1H), 8.10 (d, J = 1.8 Hz, 1H), 8.02 (d, J = 8.0 Hz, 1H), 7.87 (dd, J = 8.4, 1.8 Hz, 1H), 7.80 (d, J = 8.4 Hz, 1H), 7.72–7.68 (m, 2H), 7.63 (s, 1H), 7.51–7.47 (m, 1H), 3.34 (s, 8H), 2.94 (s, 3H); ¹³C NMR (126 MHz, DMSO-*d*₆) δ : 168.47, 157.89, 148.47, 146.52, 138.60, 135.59, 135.01, 131.93, 131.37, 130.80, 130.24, 129.12, 128.79, 127.62, 126.02, 125.74, 125.58, 121.42, 106.72, 52.94, 47.63, 42.72, 14.34; MS for C₂₄H₂₂Cl₂N₆S: [M + H]⁺ calculated m/z : 497.10 and observed: 497.2287.

2.3.8. (E)-4-(4-fluorophenyl)-2-(2-((2-(4-methylpiperazin-1-yl)quinolin-3-yl)methylene)hydrazineyl)thiazole (6g). FT-IR (cm⁻¹): 3176, 3105, 2920, 2854, 1590, 1558, 1485, 1354, 1277, 1154, 1089, 983, 836, 794, 684, 520; ¹H NMR (500 MHz, DMSO-*d*₆) δ : 12.35 (s, 1H), 8.58 (s, 1H), 8.23 (s, 1H), 8.05–8.01 (m, J = 7.3 Hz, 1H), 7.92 (m, 2H), 7.82–7.79 (m, 1H), 7.72–7.68 (m, 1H), 7.49 (t, J = 7.3 Hz, 1H), 7.39 (s, 1H), 7.29–7.24 (m, 2H), 3.33 (s, 8H), 2.93 (s, 3H); ¹³C NMR (126 MHz, DMSO-*d*₆) δ : 167.76, 161.55 (d, J = 244.5 Hz), 157.35, 149.48, 145.93, 137.73, 134.34, 131.12, 130.20, 128.21, 127.41 (d, J = 8.1 Hz), 127.07, 125.17, 125.04, 120.95, 115.40 (d, J = 21.5 Hz), 103.65, 52.38, 47.06, 42.16; MS for



$C_{24}H_{23}FN_6S$: $[M + H]^+$ calculated m/z : 447.17 and observed: 447.2705.

2.3.9. (E)-4-(2-((2-(4-methylpiperazin-1-yl)quinolin-3-yl)methylene)hydrazineyl)thiazol-4-yl)benzonitrile (6h). FT-IR (cm^{-1}): 3418, 3195, 3116, 3038, 2844, 2217, 1606, 1486, 1436, 1361, 1281, 1161, 1122, 1051, 984, 841, 782, 670, 518; 1H NMR (500 MHz, $DMSO-d_6$) δ : 12.42 (s, 1H), 8.59 (s, 1H), 8.24 (s, 1H), 8.06 (d, $J = 8.3$ Hz, 2H), 8.04–8.00 (m, 1H), 7.89 (d, $J = 8.3$ Hz, 2H), 7.82–7.79 (m, 1H), 7.74–7.68 (m, 2H), 7.51–7.47 (m, 1H), 3.35 (s, 8H), 2.93 (s, 3H); ^{13}C NMR (126 MHz, $DMSO-d_6$) δ : 168.57, 157.90, 149.34, 146.51, 139.12, 138.67, 135.04, 133.21, 130.83, 128.80, 127.62, 126.59, 125.76, 125.58, 121.43, 119.46, 110.13, 108.35, 52.94, 47.63, 42.73; MS for $C_{24}H_{23}FN_6S$: $[M + H]^+$ calculated m/z : 454.18 and observed: 454.2892.

2.4. MTT assay on MDA-MB-231 cells

A cytotoxicity assay of the synthesized compounds was performed against the triple-negative breast cancer cell line MDA-MB-231 (NCCS, Pune; passage 52) using the MTT colorimetric method. Cells were maintained in MEM supplemented with 10% fetal bovine serum, 1% antibiotic-antimycotic, and 1.25 mM HEPES, and seeded at 10 000 cells/well in 96-well plates and allowed to adhere for 24 h at 37 °C in a 5% CO_2 incubator. Test compounds and reference drugs like doxorubicin, 5-FU, gefitinib, ceritinib were prepared in DMSO as stock solutions and diluted in complete medium to final concentrations of 1, 2, 4, 8, and 16 μM (final DMSO $\leq 0.5\%$ v/v) and added in triplicate; vehicle and untreated controls were included. After 24 h treatment, 25 μL of MTT (5 mg mL^{-1} in PBS) was added to each well (final MTT ~ 0.42 mg mL^{-1}) and incubated for 2–3 h at 37 °C. Formazan crystals were dissolved in 100 μL DMSO and absorbance read at 570 nm. Percent viability was calculated relative to vehicle control and IC_{50} values determined by nonlinear regression (four-parameter logistic fit) from at least three independent experiments. [note: MTT (3-(4,5-dimethylthiazol-2-yl)-2,5-diphenyltetrazolium bromide), MDA-MB-231 (triple-negative human breast cancer cell line), NCCS (national centre for cell science), MEM (minimum essential medium), FBS (fetal bovine serum), HEPES (4-(2-hydroxyethyl)-1-piperazineethanesulfonic acid), PBS (phosphate buffered saline), EDTA (ethylenediaminetetraacetic acid), CO_2 (carbon dioxide), DMSO (dimethyl sulfoxide), IC_{50} (half maximal inhibitory concentration), μM (micromolar), μL (microliter), nm (nanometer)]

2.5. Molecular docking

The 3D crystal structure of EGFR (PDB ID: 1M17 (<https://www.rcsb.org/structure/1M17>)) was obtained from the Protein Data Bank and prepared using AutoDock Tools v1.5.6, as previously described.⁵³ Ligands were energy-minimized at the MM2 level using Chem3D Pro⁵⁴ to ensure structural stability. Docking was performed with AutoDock Vina v1.2.0, employing a hybrid Lamarckian Genetic Algorithm and empirical scoring function. Water molecules were removed, hydrogens added, and Kollman charges assigned. Docking used with a $70 \times 70 \times 70$ Å grid centered on the AQ4-binding site ($x = 20.143$, $y =$

0.376 , $z = 52.218$) and exhaustiveness of 8. Protocol validation by re-docking the native ligand yielded an RMSD < 2.0 Å. Visualization was done using Discovery Studio Visualizer v16.1.0.⁵⁵

2.6. Swiss ADME prediction

In silico ADME analysis of the synthesized compounds was performed using the SwissADME web tool (<http://www.swissadme.ch/>).⁵⁶ The SMILES notations of each compound were input to predict key pharmacokinetic and drug-likeness parameters. Physicochemical descriptors such as topological polar surface area (TPSA), number of hydrogen bond donors/acceptors, and rotatable bonds were evaluated. Lipophilicity was assessed using the consensus log P value, and aqueous solubility was predicted *via* the ESOL and SILICOS-IT models. Pharmacokinetic properties profiles were analyzed. Drug-likeness was determined based on Lipinski's rule of five.

3. Results and discussion

3.1. Chemistry and spectral discussion

The synthetic strategy toward the thiazole–quinoline hybrid molecules (**6a–6h**) involved a well-planned multistep procedure beginning with the Vilsmeier–Haack formylation of *N*-acetylaniline to furnish a 2-chloroquinoline-3-carbaldehyde intermediate (compound **2**). This reaction utilized $POCl_3$ and DMF under promoting electrophilic substitution followed by ring closure and formylation at the C-3 position. The intermediate **2** was then subjected to nucleophilic aromatic substitution with *N*-methylpiperazine in the presence of K_2CO_3 , 2-(4-methylpiperazin-1-yl)quinoline-3-carbaldehyde (**3**). This carbaldehyde was then employed in a one-pot cyclocondensation reaction with thiosemicarbazide (**4**) and substituted phenacyl bromides (**5a–5h**) in PEG-400 solvent and sulfamic acid to form the final thiazole–quinoline hybrids (**6a–6h**). The mechanism involves initial formation of a thiosemicarbazone followed by thiazole ring cyclization *via* nucleophilic attack and elimination of bromide. The structural diversity of the final hybrids arises from various electron-donating and electron-withdrawing groups on the phenacyl bromides (Table 1), thus tailoring their potential biological activities. The synthesized compounds were characterized comprehensively using FT-IR, 1H and ^{13}C NMR spectroscopy and Mass spectrometry. In FT-IR, the NH peaks in the synthesized compounds were found at 3418 – 3148 cm^{-1} , the aromatic C–H appears near 3105 – 3044 cm^{-1} , and the aliphatic C–H near 2983 – 2839 cm^{-1} . The azomethine C=N stretch is prominent in the 1648 – 1590 cm^{-1} region. Characteristic peaks for various substituents are also observed in their corresponding spectra. The aldehyde precursor **3** shows the expected formyl singlet at δ 10.18, quinoline aromatics at δ ~ 8.5 – 7.3 , piperazine methylenes as two multiplet envelopes (δ 3.59–3.50 and 2.70–2.61, 8H total), and the $N-CH_3$ at δ 2.39. For **6a–6h**, a downfield singlet at δ ~ 12.47 – 12.31 (1H) corresponds to the hydrazone NH, and a singlet near δ 8.25 (1H) to the azomethine CH. Quinoline/arene protons appear between δ ~ 8.6 – 7.3 with patterns reflecting substituents: **6a** (4- NO_2) shows the pair at δ 8.30/8.14 (2H each); **6b/6c** (4-Br/4-Cl) give doublets near



Table 1 Structural diversity and physicochemical data of the synthesized compounds (6a–6h)

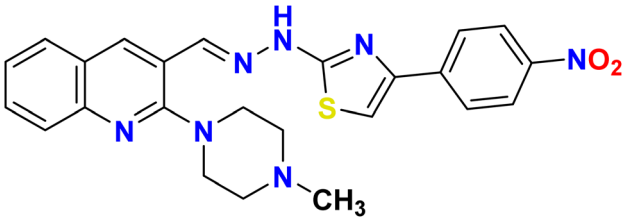
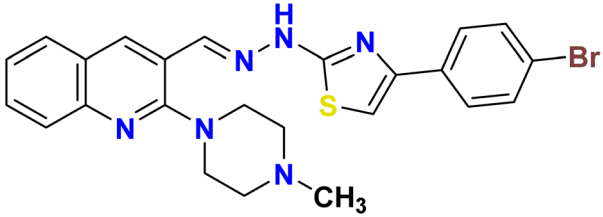
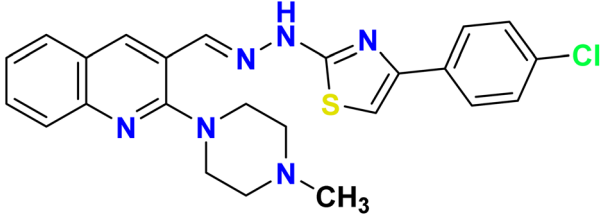
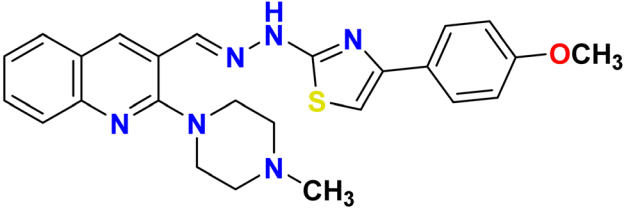
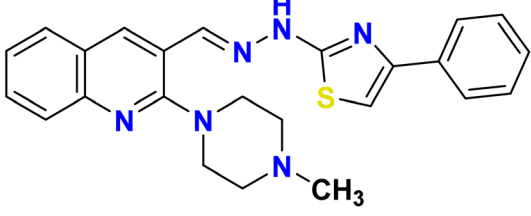
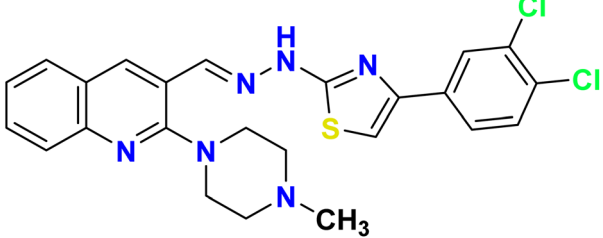
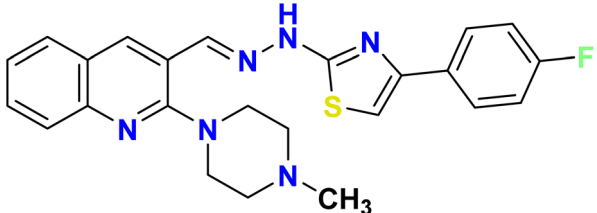
Entry	Structures	Yield (%)	M.P. (°C)
6a		92	248–250
6b		89	208–210
6c		90	204–206
6d		85	176–178
6e		82	236–238
6f		90	242–244
6g		84	236–238



Table 1 (Contd.)

Entry	Structures	Yield (%)	M.P. (°C)
6h		90	218–220

$\delta \sim 7.90/7.62$ and $\sim 7.90/7.50$, respectively; **6d** (4-OMe) has δ 3.80 (s, 3H) and para-aromatic δ 6.98 (d, 2H); **6e** (phenyl) presents multiplets across $\delta \sim 7.88\text{--}7.30$; **6f** (3,4-dichloro) shows the expected pattern; **6g** (4-F) exhibits fluorine-coupled aromatic multiplets around $\delta \sim 7.92$ and $7.29\text{--}7.24$; **6h** (4-CN) shows two para sets at δ 8.06 and 7.89 (2H each). In all **6a–6h**, the piperazine methylenes collapse to an 8H singlet near δ 3.33 and the N-CH₃ appears as a 3H singlet at $\delta \sim 2.88\text{--}2.94$. Compound **3** shows the aldehyde carbon at δ 190.27, quinoline carbons over $\delta \sim 159\text{--}122$, and piperazine/N-Me carbons at $\delta \sim 55/51/46$. For **6a–6h**, the imine C=N resonates at $\delta \sim 168\text{--}167$; quinoline/thiazole/arene quaternaries populate $\delta \sim 158\text{--}140$, with remaining aromatics in the $\delta \sim 134\text{--}120$ range. In compound **6g** (4-F) gives C-F at δ 161.55 (d, $J = 244.5$ Hz) with additional ¹⁹F-coupled carbons at δ 115.40 (d, $J = 21.5$ Hz) and 127.41 (d, $J = 8.1$ Hz). Across the series, piperazine carbons appear at $\delta \sim 52\text{--}47$ ppm and the N-methyl near $\delta \sim 42$, in agreement with tertiary amine substitution. All species show $[M + H]^+$ that agree closely with calculated values: **3** (calc 256.14, found 256.1448), **6a** (474.17/474.2784), **6b** (507.09/507.2186) with the expected bromine isotopic partner at m/z 509.2050 ($\sim 1:1$), **6c** (463.14/463.2554) plus m/z 465.2479 for ³⁷Cl ($\sim 3:1$ pattern overall for a single Cl), **6d** (459.19/459.3092), **6e** (429.18/429.2868), **6f** (497.10/497.2287) with an $[M + H + 2]^+$ at 499.2132 (due to Cl₂ giving the characteristic M/M + 2/M + 4 cluster), **6g** (447.17/447.2705), and **6h** ($[M + H]^+$ found 454.2892), all consistent with the proposed molecular formulas and substituent patterns (nitro, halogens, fluoro, methoxy, and nitrile). These spectral features confirmed the successful construction of the thiazole-quinoline scaffolds and the identity of all synthesized analogs (**6a–6h**), paving the way for their further biological evaluation.

3.2. Anti-breast cancer activity

The anti-breast cancer potential of the synthesized quinolyl-thiazole hybrid derivatives (**6a–6h**) was evaluated against the triple-negative breast cancer (TNBC) cell line MDA-MB-231 using an *in vitro* MTT cytotoxicity assay. The IC₅₀ values summarized in Table 2 indicate that most of the compounds exhibited significant cytotoxic activity. To understand the influence of structural variations on biological activity, a structure-activity relationship (SAR) analysis was conducted based on the nature and position of substituents on the aryl ring

attached to the C4-position of the thiazole core. The synthesized quinolyl-thiazole hybrid derivatives (**6a–6h**) exhibited significant cytotoxic activity against MDA-MB-231 cells, with IC₅₀ values ranging from 1.415 ± 0.16 to 2.898 ± 0.27 μ M. Among these, compound 4-nitrophenyl containing thiazole derivative (**6a**) emerged as the most potent derivative with an IC₅₀ of 1.415 ± 0.16 μ M, closely followed by **6g** (4-fluorophenyl, IC₅₀ = 1.484 ± 0.13 μ M) and **6h** (4-cyanophenyl, IC₅₀ = 1.658 ± 0.15 μ M). These results indicate that strong electron-withdrawing groups (EWGs) at the para-position of the aryl ring significantly enhance anticancer activity. In contrast, compounds **6b** (4-bromo, IC₅₀ = 2.357 ± 0.23 μ M), **6c** (4-chloro, IC₅₀ = 2.539 ± 0.26 μ M), and **6e** (unsubstituted phenyl, IC₅₀ = 2.390 ± 0.21 μ M) displayed moderate activity. Interestingly, **6d** (4-methoxy, IC₅₀ = 2.548 ± 0.29 μ M), containing an electron-donating group (EDG), also showed reduced cytotoxicity compared to EWG-bearing analogues. Compound **6f** (3,4-dichloro, IC₅₀ = 2.898 ± 0.27 μ M), featuring dual halogen substitution at the meta and para positions, was the least active among the series. When compared to standard anticancer agents, most synthesized compounds outperformed 5-fluorouracil (5-FU, IC₅₀ = 72.48 ± 6.89 μ M) and gefitinib (IC₅₀ = 35.42 ± 4.18 μ M), and were nearly as potent or comparable to ceritinib (IC₅₀ = 1.043 ± 0.098 μ M) while being significantly more active than doxorubicin (IC₅₀ = 8.23 ± 0.79 μ M). The cell morphology study of MDA-MB-231 cells treated with compounds **6a**, **6f**, **6g**, and **6h** at concentrations of 1, 2, and 4 μ M (Fig. 2) revealed significant, dose-

Table 2 Anti-Breast cancer activity on triple negative breast cancer cell line (MDA-MB-231)

Entry	IC ₅₀ (μ M)
6a	1.415 ± 0.16
6b	2.357 ± 0.23
6c	2.539 ± 0.26
6d	2.548 ± 0.29
6e	2.390 ± 0.21
6f	2.898 ± 0.27
6g	1.484 ± 0.13
6h	1.658 ± 0.15
Doxorubicin	8.23 ± 0.79
5-FU	72.48 ± 6.89
Gefitinib	35.42 ± 4.18
Ceritinib	1.043 ± 0.098



dependent cytotoxic effects. The IC_{50} values of all the listed anticancer drugs were experimentally determined to validate their inhibitory activity. As the evaluation was limited to the MTT assay, additional assays will be necessary to strengthen these biological conclusions.

3.3. Molecular docking study

In view of the *in vitro* anti-breast cancer evaluation against the triple-negative MDA-MB-231 cell line, where **6a** demonstrated the most potent cytotoxic activity ($IC_{50} = 1.415 \pm 0.16 \mu M$) followed by

6g ($IC_{50} = 1.484 \pm 0.13 \mu M$) and **6h** ($IC_{50} = 1.658 \pm 0.15 \mu M$), and **6f** exhibited comparatively lower potency ($IC_{50} = 2.898 \pm 0.27 \mu M$), molecular docking was performed for these four representative compounds to rationalize their biological profiles. All docking studies were conducted against the EGFR tyrosine kinase domain (PDB ID: 1M17) using AutoDock Tools 1.5.6. The molecular docking results of compounds **6a**, **6f**, **6g**, and **6h** with the EGFR tyrosine kinase domain (PDB ID: 1M17) are summarized in Table 3. The 3D and 2D diagrams are presented in Fig. 3–6.

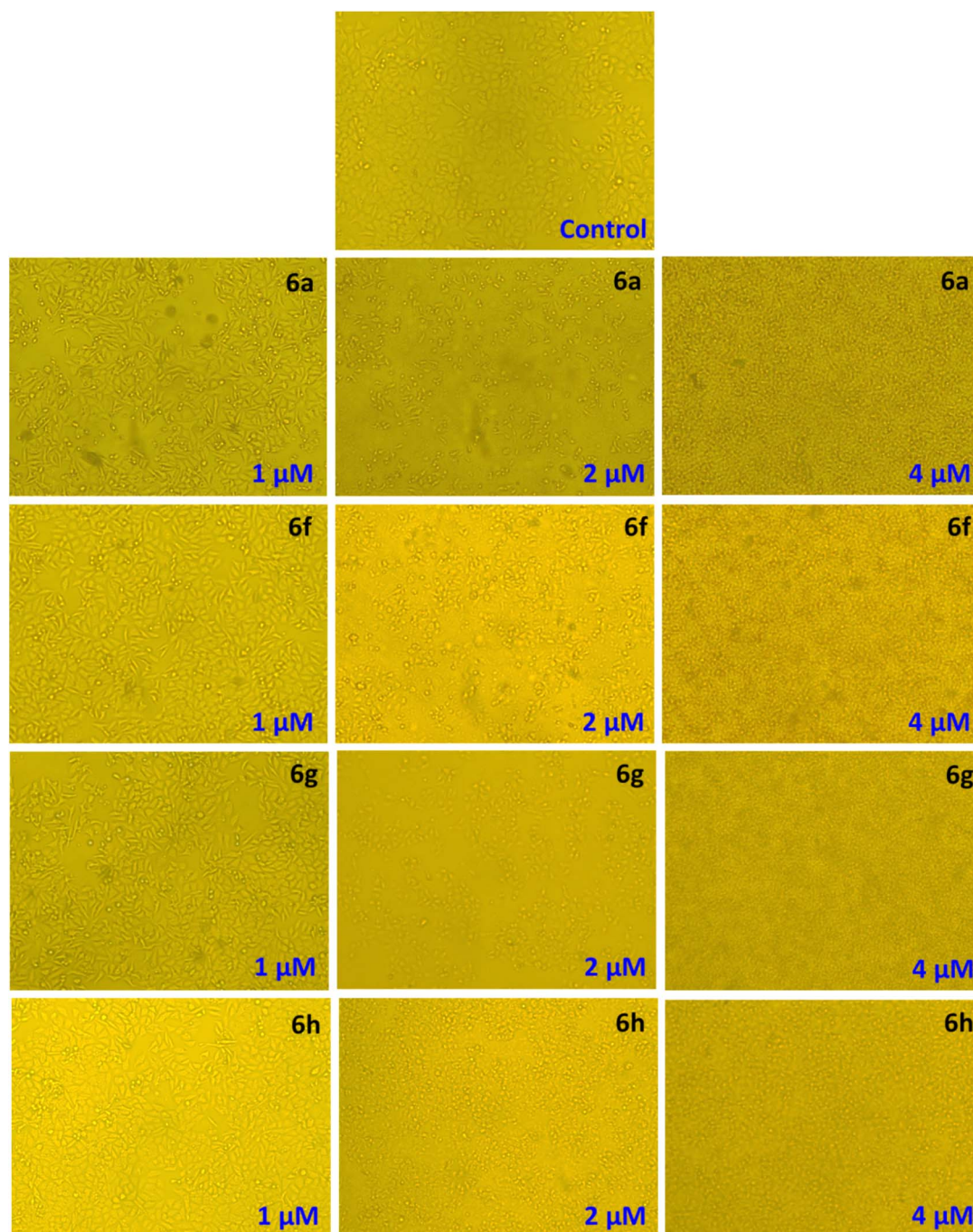


Fig. 2 Cell morphology of breast cancer cells (MDA-MB-231) treated with compounds **6a**, **6f**, **6g**, and **6h** at 1, 2, and 4 μM . Morphological changes indicate dose-dependent effects compared to the untreated control.

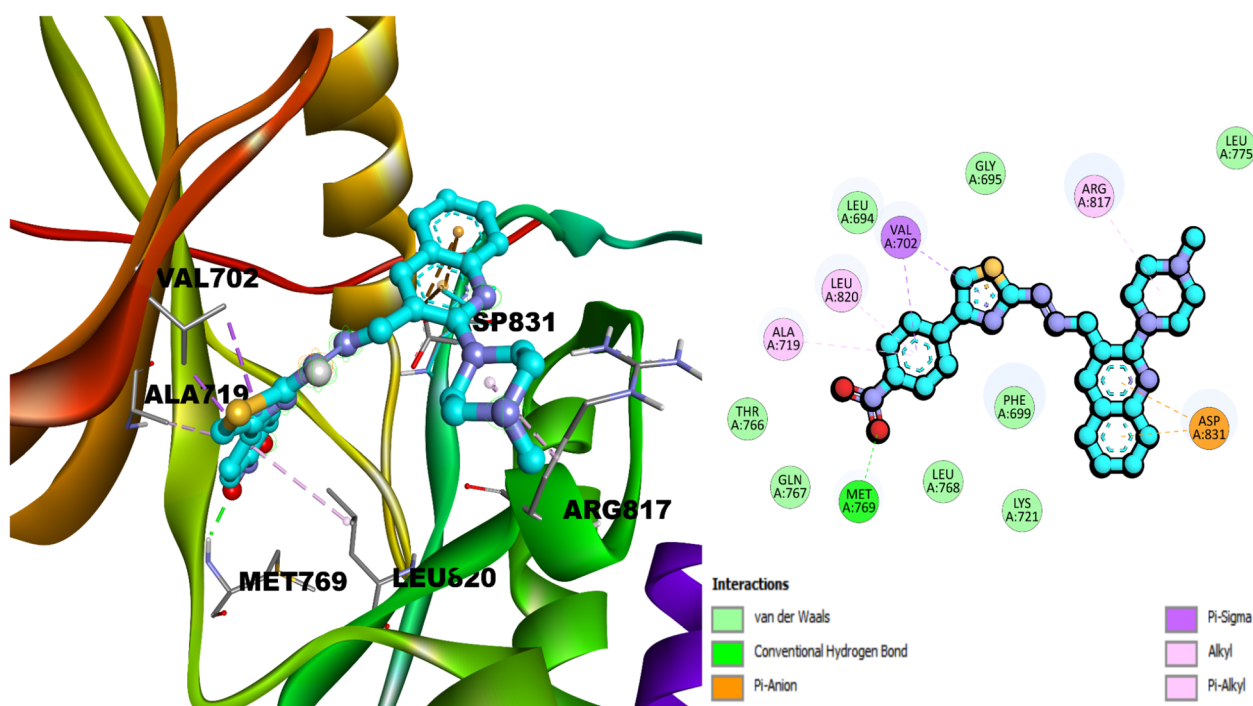


Table 3 Molecular docking scores and key binding interactions of synthesized compounds with the EGFR tyrosine kinase domain

Compound	Docking score (kcal mol ⁻¹)	Key interactions
6a	−10.0	Conventional hydrogen bond with MET769; multiple Pi–Anion interactions with ASP831; Pi–Sigma with VAL702; alkyl–alkyl with ARG817; Pi–alkyl with ALA719 and LEU820
6f	−9.2	Electrostatic interaction with ASP831; hydrogen bond with ARG817; carbon–hydrogen bond with LEU694; Pi–sigma with LEU820; Pi–alkyl with ARG817, VAL702, and ALA719
6g	−9.5	Electrostatic interaction with ASP831; hydrogen bond with SER696; halogen bonds with GLY695 and SER696; hydrogen bond with ARG817; carbon–hydrogen bond with LEU694; Pi–sigma with LEU820; Pi–alkyl with ARG817, VAL702, and ALA719
6h	−9.4	Electrostatic interaction with ASP831; hydrogen bond with SER696; halogen bonds with GLY695 and SER696; hydrogen bond with ARG817; carbon–hydrogen bond with LEU694; Pi–sigma with LEU820; Pi–alkyl with ARG817, VAL702, and ALA719

Molecular docking of the synthesized compound **6a** with the EGFR tyrosine kinase produced favourable docking score (−10.0 kcal mol⁻¹), indicating strong binding affinity. The ligand formed a key conventional hydrogen bond with the backbone amide of MET769, a critical residue involved in ATP binding.⁵⁵ In addition, the ligand established multiple Pi–anion electrostatic interactions with the negatively charged carboxylate oxygen of ASP831, which stabilized the aromatic moiety through strong electrostatic attraction. Hydrophobic

interactions further contributed to complex stabilization, including Pi–sigma contacts between the ligand's aromatic ring and the C–H groups of VAL702, an alkyl–alkyl interaction with ARG817, and Pi–alkyl contacts with the side chains of ALA719 and LEU820. These non-covalent interactions collectively enhanced shape complementarity and van der Waals stabilization in the active site. The combination of a strong hydrogen bond with MET769, multiple electrostatic interactions with ASP831, and extensive hydrophobic contacts accounts for the

**Fig. 3** Interaction of compound **6a** with EGFR tyrosine kinase.

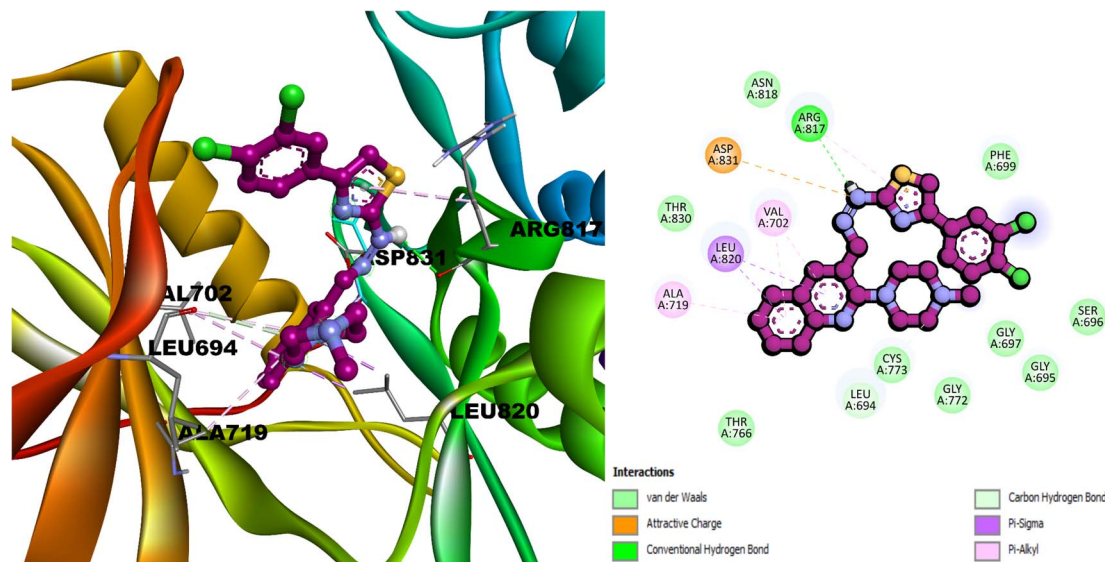


Fig. 4 Interaction of compound **6f** with EGFR tyrosine kinase.

high binding affinity, supporting the potential of compound **6a** as a potent EGFR inhibitor with promising activity against the triple-negative MDA-MB-231 breast cancer cell line. The docking analysis of compound **6g** revealed a docking score of $-9.5 \text{ kcal mol}^{-1}$, indicating strong binding affinity. The ligand formed multiple stabilizing interactions within the active site, starting with an electrostatic attractive charge between the positively charged nitrogen of the ligand and the negatively charged side chain oxygen of ASP831. A key dual-interaction motif was observed where the fluorine atom of the ligand established both a conventional hydrogen bond with the amide hydrogen of SER696 and halogen bonding with GLY695 and SER696, enhancing specificity. Additionally, the ligand engaged in a conventional hydrogen bond *via* its imine hydrogen with

the carbonyl oxygen of ARG817 and a carbon hydrogen bond between a ligand carbon and the backbone oxygen of LEU694. Hydrophobic interactions further stabilized the complex, including Pi-sigma interactions with LEU820 and Pi-alkyl contacts with ARG817, VAL702, and ALA719. The combination of electrostatic, hydrogen-bond, halogen-bond, and hydrophobic interactions positions **6g** favourably within the active site, supporting its EGFR inhibitory potential. Docking of compound **6h** afforded a score of $-9.4 \text{ kcal mol}^{-1}$; when we docked **6h** into the active site of the target protein. An electrostatic attractive-charge interaction is observed between a positively charged ligand nitrogen and the carboxylate oxygen of ASP831, helping to orient the scaffold toward the catalytic cleft. A notable dual motif around the ligand's halogen (F) reinforces

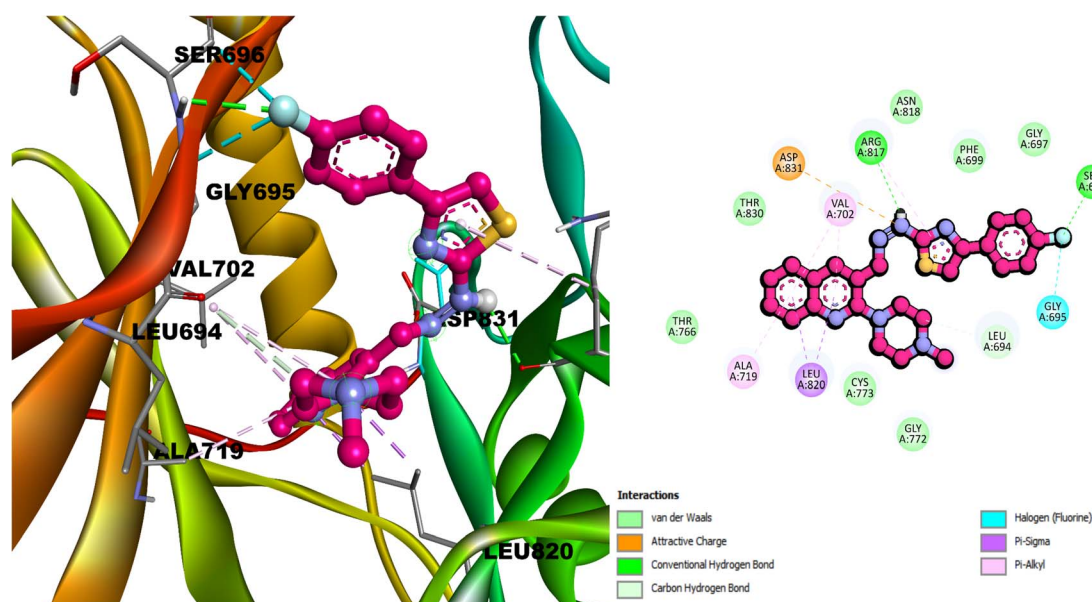


Fig. 5 Interaction of compound **6g** with EGFR tyrosine kinase.



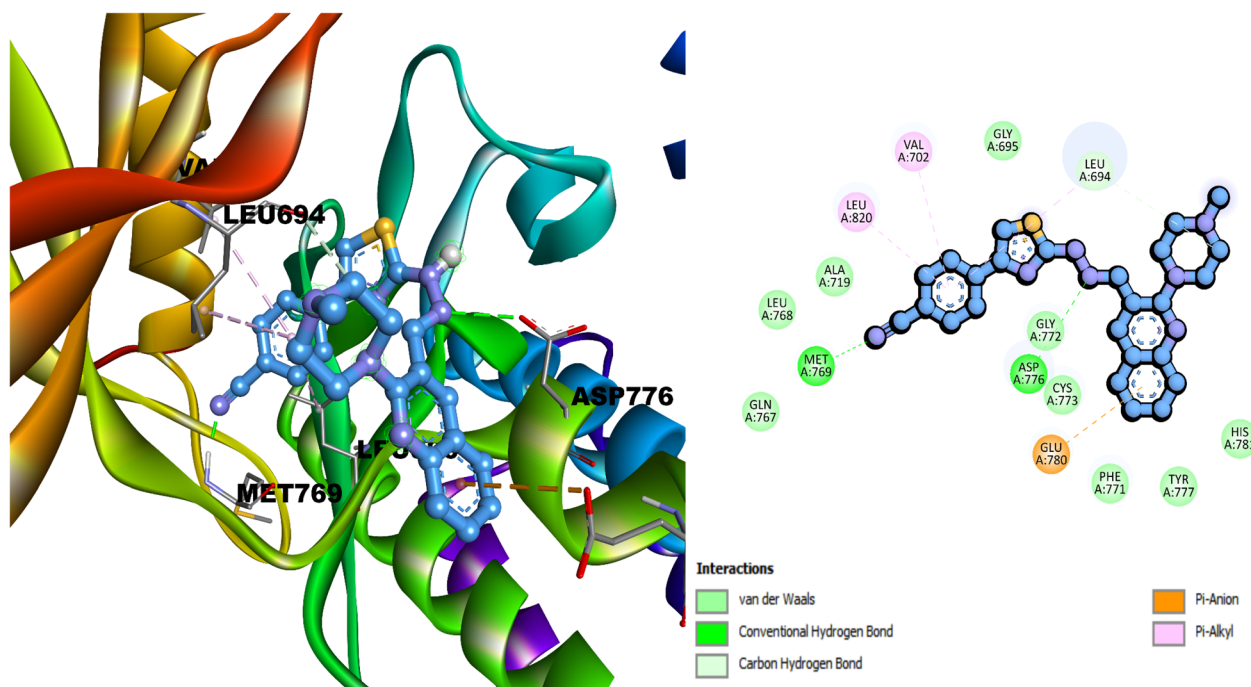


Fig. 6 Interaction of compound **6h** with EGFR tyrosine kinase.

anchoring at the entrance region: a conventional H-bond between SER696–HN and the ligand F contact together with halogen bonds to GLY695 and SER696. Additional polarity is provided by a conventional hydrogen bond from a ligand N–H to ARG817 and a carbon–hydrogen bond from a ligand carbon to LEU694. The pose is further consolidated by a cluster of hydrophobic contacts: Pi–sigma interactions with LEU820 and multiple Pi–alkyl contacts to ARG817, VAL702, and ALA719. Together, contacts with ASP831, SER696, and GLY695, supported by hydrophobic interactions, account for the favourable binding of **6h** to EGFR. The least potent, compound **6f** had a docking score of $-9.2 \text{ kcal mol}^{-1}$ with electrostatic, hydrogen-bond, and hydrophobic interactions in the EGFR active site. A key electrostatic attractive-charge contact is formed between the positively charged ligand nitrogen and the carboxylate oxygen of ASP831, which likely assists in orienting the ligand. This is complemented by a conventional hydrogen bond from a ligand N–H to ARG817 and a carbon–hydrogen bond between a ligand carbon and LEU694. Additional stabilization arises from Pi–sigma hydrophobic interactions with LEU820, alongside multiple Pi–alkyl contacts to ARG817, VAL702 and ALA719. These interactions collectively generate a robust hydrophobic network surrounding the ligand's aromatic core, while the electrostatic and hydrogen-bond contacts help lock the scaffold in an orientation favourable for kinase inhibition, rationalizing the strong binding affinity of **6f**. Among the docked compounds, the most potent **6a** also exhibited the highest binding affinity, while the least potent **6f** showed the lowest docking score, thereby validating the docking results against the observed cytotoxicity trends. Similarly, **6g** and **6h**, with intermediate IC_{50} values, displayed correspondingly strong but slightly lower binding affinities than **6a**. In line with *in vitro*

cytotoxicity results against MDA-MB-231 cells, compound **6a**, the most potent ($\text{IC}_{50} = 1.415 \pm 0.16 \mu\text{M}$), showed the strongest docking score ($-10.0 \text{ kcal mol}^{-1}$) and distinct interactions. In contrast, the less potent **6f** ($\text{IC}_{50} = 2.898 \pm 0.27 \mu\text{M}$) lacked this key hydrogen bond with MET769 and relied primarily on weaker interactions such as carbon–hydrogen bonding with LEU694 and electrostatic contact with ASP831. Compounds **6g** and **6h**, with intermediate potency, featured halogen bonds (with GLY695 and SER696) and shared hydrogen bonding with ARG817, yet did not engage MET769. These findings suggest that hydrogen bonding with MET769 and Pi–anion interactions with ASP831 may contribute significantly to enhanced binding affinity and biological activity. This parallel between experimental potency and predicted binding strength underscores the relevance of the docking analysis in explaining the EGFR inhibitory potential of these compounds against the MDA-MB-231 cell line. The re-docking validation of erlotinib into the EGFR (1M17) binding site (RMSD 1.524 \AA) is given in Fig. 7. Although a good correlation between IC_{50} values and docking scores against EGFR was observed, the absence of a direct enzymatic assay limits definitive confirmation of EGFR inhibition in this study. Importantly, Molecular docking results are predictive in nature, and further biochemical assays are required to confirm EGFR as the target.

3.4. ADME study

The ADME and drug likeness profiles of compounds **6a–6h** were analyzed to assess their pharmacological potential (Table 4) using SwissADME online tool.⁵⁶ Compounds **6a–6h** showed a range of TPSA values $84.89\text{--}130.71 \text{ \AA}^2$. All compounds possessed one hydrogen bond donor and 4–6 acceptors, which were enough targets polarity. Flexibility was ensured by up to 5–

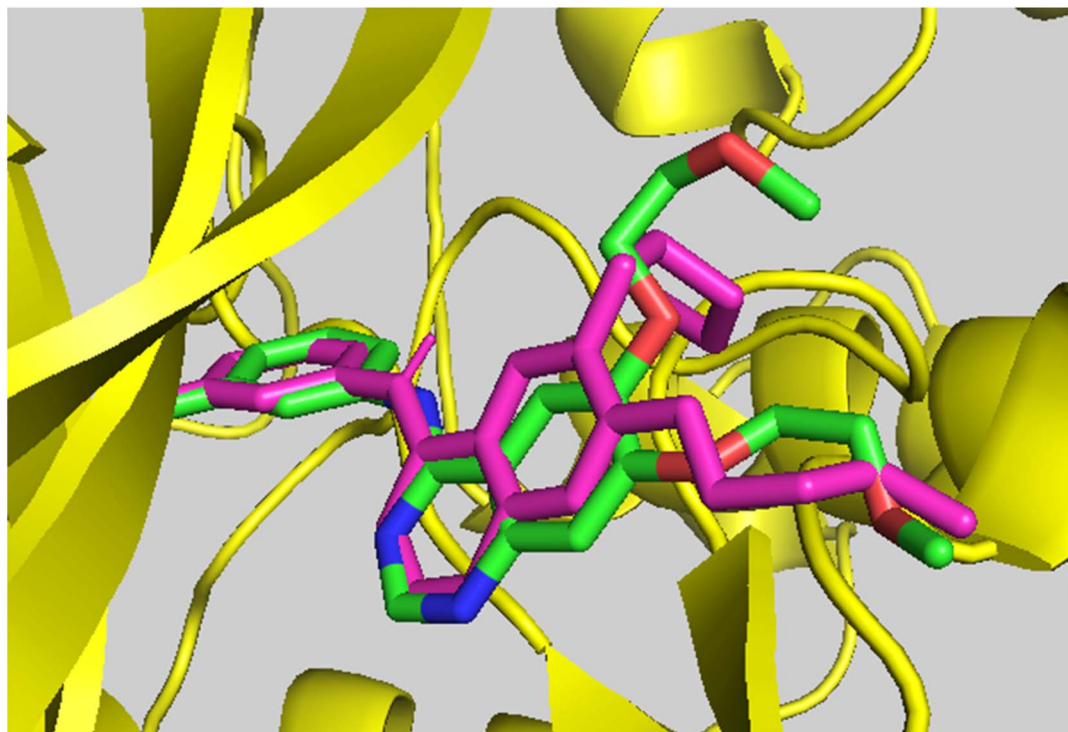


Fig. 7 Re-docking validation of erlotinib into the EGFR (1M17) binding site (RMSD 1.524 Å).

6 rotatable bonds. Log $P_{o/w}$ values varied from 3.15 (**6a**) to 5.08 (**6f**), and the obtained values pointed to moderate to high lipophilicity. The water solubility (log S , ESOL) ranged among **6a**, **6d**, **6e**, and **6h** being moderately soluble and others especially **6f** were poorly soluble. All compounds showed high GI absorption and categorization as non-BBB permeant, which is favorable for non-CNS targets. P-gp substrate prediction was negative only for **6a** for being better retained, while **6b–6h** might suffer from efflux. All were metabolically inhibitory for CYP2C19 and CYP2C9, and all but **6a** and **6f** were also inhibitory for CYP2D6

and CYP3A4. All the compounds obeyed the Veber rule and only **6b** slightly violated Lipinski's rule (high molecular weight). There was no PAINS alert, so there were little assay interferences. Brenk warnings highlighted one imine group in **6b–6h** and three warnings in **6a**. Graphical ADME profiling of the compounds (**6a–6h**) is given Table S1 (SI). The ADME results presented are based on *in silico* predictions and require further experimental validation, including solubility, serum stability, and metabolic stability studies.

Table 4 *In Silico* ADME, drug likeness, and medicinal chemistry properties of compounds **6a–6h**^a

Category	Parameter	6a	6b	6c	6d	6e	6f	6g	6h
Physicochemical	TPSA (Å ²)	130.71	84.89	84.89	94.12	84.89	84.89	84.89	108.68
	H-bond donors	1	1	1	1	1	1	1	1
	H-bond acceptors	6	4	4	5	4	4	5	5
	Rotatable bonds	6	5	5	6	5	5	5	5
Lipophilicity	Consensus log $P_{o/w}$	3.15	4.57	4.50	3.92	3.95	5.08	4.28	3.76
Water Solubility	log S (ESOL)	−5.94	−6.79	−6.48	−5.95	−5.88	−7.07	−6.04	−5.83
Pharmacokinetics	GI absorption	High	High	High	High	High	High	High	High
	BBB permeant	No	No	No	No	No	No	No	No
	P-gp substrate	No	Yes	Yes	Yes	Yes	Yes	Yes	Yes
	CYP2C19 inhibitor	Yes	Yes	Yes	Yes	Yes	Yes	Yes	Yes
	CYP2C9 inhibitor	Yes	Yes	Yes	Yes	Yes	Yes	Yes	Yes
	CYP2D6 inhibitor	No	Yes	Yes	Yes	Yes	No	Yes	Yes
	CYP3A4 inhibitor	Yes	Yes	Yes	Yes	Yes	No	Yes	Yes
Druglikeness	Lipinski rule	Yes (0)	Yes (1)	Yes (0)	Yes (0)	Yes (0)	Yes (0)	Yes (0)	Yes (0)
	Veber rule	Yes	Yes	Yes	Yes	Yes	Yes	Yes	Yes
Med. Chemistry	PAINS filter	0 alerts	0 alerts	0 alerts	0 alerts	0 alerts	0 alerts	0 alerts	0 alert
	Brenk alerts	3 (imine, nitro, O–N)	1 (imine_1)	1 (imine_1)	1 (imine_1)	1 (imine_1)	1 (imine_1)	1 (imine_1)	1 (imine_1)

^a Note: full forms of the abbreviations used in this table are provided in the SI.



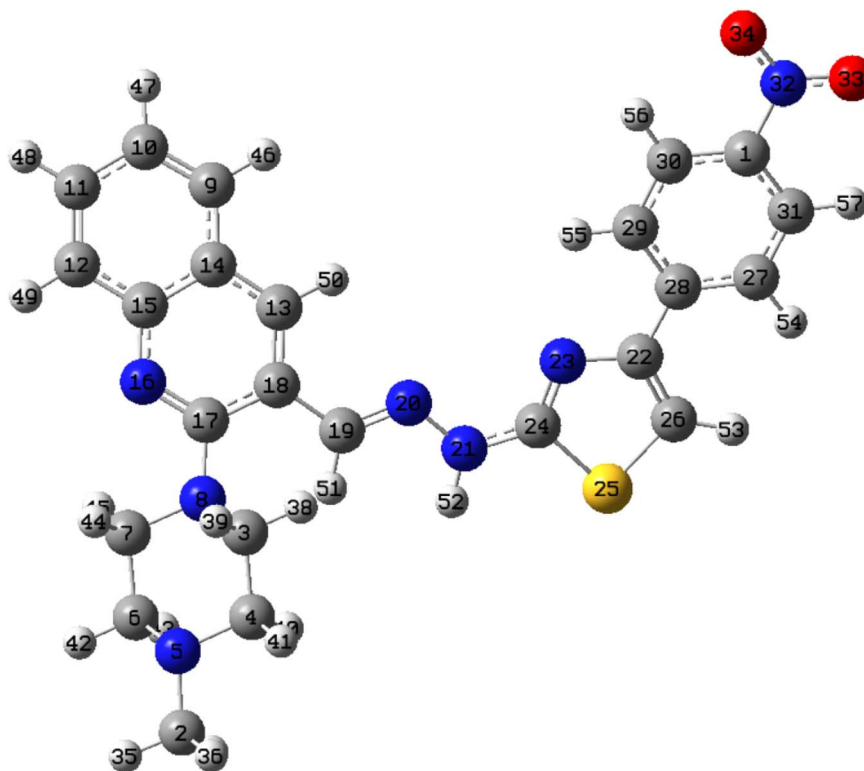


Fig. 8 Optimized molecular geometry of compound **6a** obtained using DFT (B3LYP/6–31++G(d,p)) level, showing planar conjugation across the quinoline–hydrazone–thiazole–nitrophenyl core and a non-planar piperazine ring (nitrogen in blue, oxygen in red, sulfur in yellow, carbon in grey and hydrogen atoms in white colors).

3.5. DFT calculations

DFT has emerged as a powerful computational approach for investigating the electronic structure, chemical stability, and reactivity profiles of a wide range of small organic molecules. This method provides valuable theoretical insights that support

experimental findings and aid in the rational design of compounds for chemical and pharmacological applications.^{57–59} In the present study, calculations for the compound **6a** were performed in the gas phase using the Gaussian 03 computational package.⁶⁰ The electronic properties were evaluated using the B3LYP functional, which combines Becke's three-parameter

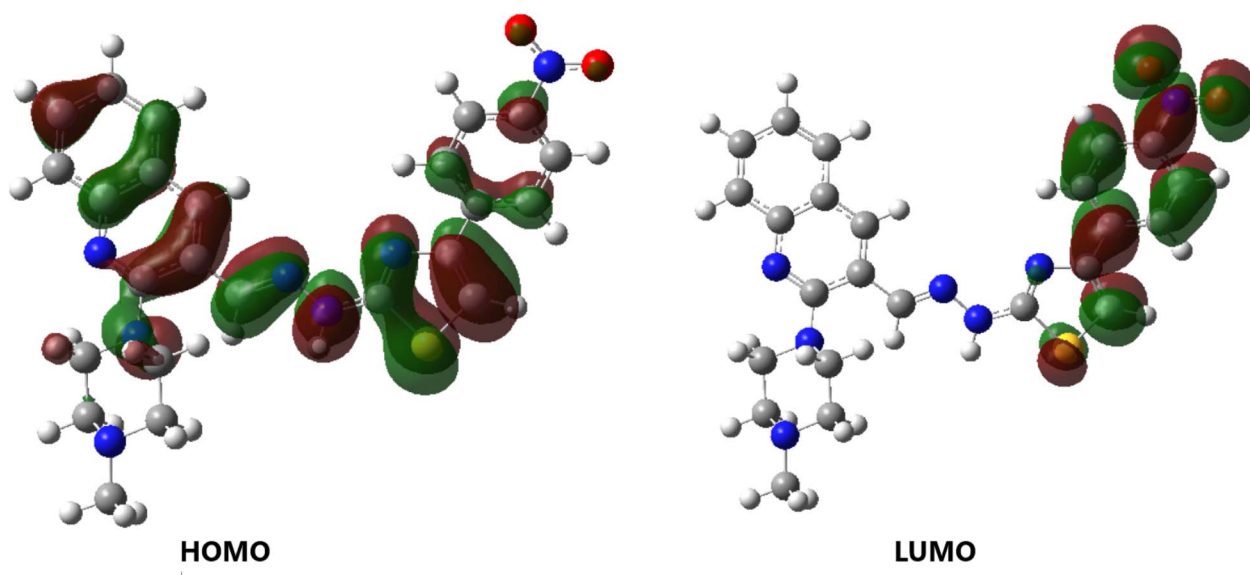


Fig. 9 The frontier molecular orbitals (FMO) of compound **6a** obtained using DFT (B3LYP/6–31++G(d,p)) level (nitrogen in blue, oxygen in red, sulfur in yellow, carbon in grey and hydrogen atoms in white colors).

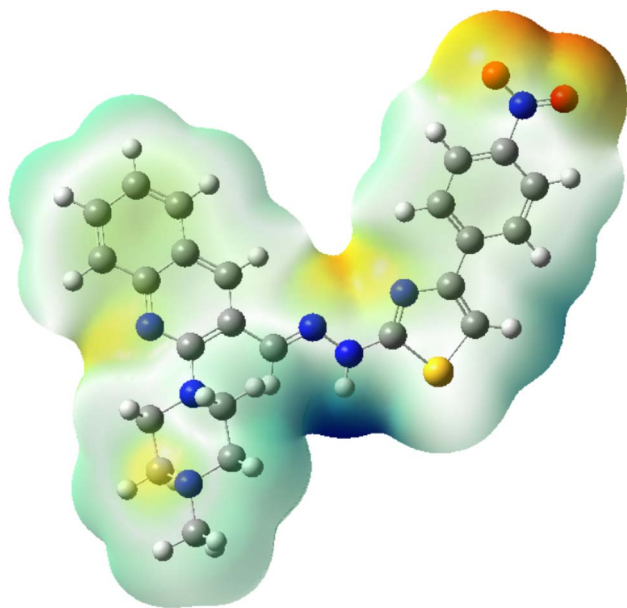


Fig. 10 MESP Plot of the compound **6a** obtained using DFT (B3LYP/6-31++G(d,p)) level (nitrogen in blue, oxygen in red, sulfur in yellow, carbon in grey and hydrogen atoms in white colors).

exchange functional with the Lee–Yang–Parr correlation functional,^{61,62} in conjunction with the 6-31++G(d,p) basis set. Visualization and interpretation of the optimized molecular geometries and frontier molecular orbitals were facilitated using the GaussView version 4.1.2 graphical interface.⁶³ The DFT-optimized structure (Fig. 8) on B3LYP/6-31++G(d,p) level for compound **6a** showed that there is an almost planar conjugated plane over the quinoline, hydrazone, thiazole, and nitrophenyl groups. The piperazine ring takes a non-planar chair conformation adding flexibility and facilitating binding contacts. The frontier molecular orbitals (FMO) of compound **6a** are shown in Fig. 9. The HOMO of molecule **6a** is mainly distributed over the quinoline, hydrazone, and thiazole rings, which indicates the strong π -conjugation. In contrast instead, the LUMO is chiefly localized on the nitrophenyl ring, with a small contribution from the thiazole that shows the above-mentioned electron-accepting characters. MESP plot of the compound **6a** (Fig. 10) showed a negative potential (red/orange) around the nitro group and positive potential (blue) around the hydrazone and in the vicinity of the piperazine nitrogen atoms. The total charge distribution indicates a polar molecule capable of intramolecular charge transfer and potential interaction with the biological targets.

4 Conclusion

The present study successfully designed, synthesized, and characterized a novel series of quinolinyl-thiazole derivatives incorporating an *N*-methyl piperazine moiety, which demonstrated potent activity against the triple-negative breast cancer cell line MDA-MB-231. The use of PEG-400 and sulfamic acid offered an environmentally benign approach. Among them, compound **6a** was found to be the most promising candidate, exhibiting the lowest IC₅₀ value and the strongest binding affinity toward the

EGFR tyrosine kinase domain, as supported by molecular docking analysis. The correlation between experimental cytotoxicity and predicted binding energies suggests EGFR as a potential target that warrants further investigation. Additionally, favorable *in silico* ADME and drug-likeness profiles, along with DFT based structural and electronic characteristics provided additional insights.

Author contributions

Archana B. Dhongade: Contributed to the design of the synthetic methodology, carried out the synthesis of target compounds, and performed detailed spectral characterization; Umang Shah: Conducted anticancer activity studies, analyzed biological data, and assisted in interpreting the results; Bhausaheb N. Patil: Assisted in spectral characterization, interpretation of NMR/IR/MS data, and validation of compound structures; Rahul A. Shinde: Performed molecular docking and DFT studies, provided computational insights; Ruma Sarkar: Involved in performing anticancer activity assays and biological evaluation of compounds; Adrija Mukherjee: Involved in performing anticancer activity assays and biological evaluation of compounds; Suraj N. Mali: Data interpretation; Vishnu A. Adole: Conceptualized the overall study, prepared and organized the manuscript; Thansing B. Pawar: Provided overall supervision of the research work and proofreading of the manuscript. All authors have read and approved the final version of the manuscript.

Conflicts of interest

The authors declare that there is no conflict of interest regarding the publication of this paper.

Data availability

All data generated or analysed during this study are included in this published article and its supplementary information (SI). Supplementary information: contains FT-IR, ¹HNMR, ¹³C NMR and Mass spectral copies along with compound structure (Fig. S1 to S40), ADME profiling of the compounds (**6a–6h**) (Table S1) and abbreviations and full forms from Table 1. See DOI: <https://doi.org/10.1039/d5ra06350g>.

Acknowledgements

The authors are grateful to the Research Centre in Chemistry, Loknete Vyankatrao Hiray Arts, Science and Commerce College, Panchavati, Nashik and Department of Chemistry, Mahatma Gandhi Vidyamandir's Maharaja Sayajirao Gaikwad Arts, Science and Commerce College, Malegaon for providing the necessary research facilities. We also acknowledge Central Instrumentation Facility, Savitribai Phule Pune University, Pune, for spectral analysis.



References

- 1 L. Wilkinson and T. Gathani, Understanding breast cancer as a global health concern, *Br. J. Radiol.*, 2022, **95**(1130), 20211033.
- 2 S. C. Houghton and S. E. Hankinson, Cancer progress and priorities: breast cancer, *Cancer Epidemiol. Biomarkers Prev.*, 2021, **30**(5), 822–844.
- 3 L. A. Torre, F. Islami, R. L. Siegel, E. M. Ward and A. Jemal, Global cancer in women: burden and trends, *Cancer Epidemiol. Biomarkers Prev.*, 2017, **26**(4), 444–457.
- 4 M. Baliu-Piqué, A. Pandiella and A. Ocana, Breast cancer heterogeneity and response to novel therapeutics, *Cancers (Basel)*, 2020, **12**(11), 3271.
- 5 R. Mahmoud, P. Ordóñez-Morán and C. Allegrucci, Challenges for triple negative breast cancer treatment: defeating heterogeneity and cancer stemness, *Cancers (Basel)*, 2022, **14**(17), 4280.
- 6 I. Dagogo-Jack and A. T. Shaw, Tumour heterogeneity and resistance to cancer therapies, *Nat. Rev. Clin. Oncol.*, 2018, **15**(2), 81–94.
- 7 M. Rahman, O. Afzal, S. N. M. N. Ullah, M. Y. Alshahrani, A. G. Alkhathami, A. S. A. Altamimi, *et al.*, Nanomedicine-based drug-targeting in breast cancer: pharmacokinetics, clinical progress, and challenges, *ACS Omega*, 2023, **8**(51), 48625–48649.
- 8 D. Iacopetta, J. Ceramella, N. Baldino, M. S. Sinicropi and A. Catalano, Targeting breast cancer: An overlook on current strategies, *Int. J. Mol. Sci.*, 2023, **24**(4), 3643.
- 9 X. Xiong, L. W. Zheng, Y. Ding, Y. F. Chen, Y. W. Cai, L. P. Wang, *et al.*, Breast cancer: pathogenesis and treatments, *Signal Transduct. Targeted Ther.*, 2025, **10**(1), 49.
- 10 M. H. A. Al-Jumaili, E. A. Bakr, M. A. Huessien, A. S. Hamed and M. J. Muhaidi, Development of heterocyclic-based anticancer agents: A comprehensive review, *Heterocycl. Commun.*, 2025, **31**(1), 20220179.
- 11 T. Biswas, R. K. Mittal, V. Sharma and M. I. Kanupriya, Nitrogen-fused heterocycles: Empowering anticancer drug discovery, *Med. Chem.*, 2024, **20**(4), 369–384.
- 12 A. F. Kassem, R. H. Althomali, M. M. Anwar and W. I. El-Sofany, Thiazole moiety: A promising scaffold for anticancer drug discovery, *J. Mol. Struct.*, 2024, **1303**, 137510.
- 13 A. Saxena, S. Majee, D. Ray and B. Saha, Inhibition of cancer cells by quinoline-based compounds: A review with mechanistic insights, *Bioorg. Med. Chem.*, 2024, 117681.
- 14 A. Petrou, M. Fesatidou and A. Geronikaki, Thiazole ring—a biologically active scaffold, *Molecules*, 2021, **26**(11), 3166.
- 15 M. A. Alam, Thiazole, a privileged scaffold in drug discovery, in *Privileged Scaffolds in Drug Discovery*, Academic Press, 2023, p. 1–19.
- 16 S. Kaur, K. Kaur and V. Jaitak, Thiazole and related heterocyclic systems as anticancer agents: a review on synthetic strategies, mechanisms of action and SAR studies, *Curr. Med. Chem.*, 2022, **29**(29), 4958–5009.
- 17 T. I. de Santana, M. de Oliveira Barbosa, P. A. T. de Moraes Gomes, A. C. N. da Cruz, T. G. da Silva and A. C. L. Leite, Synthesis, anticancer activity and mechanism of action of new thiazole derivatives, *Eur. J. Med. Chem.*, 2018, **144**, 874–886.
- 18 A. O. El-Abd, S. M. Bayomi, A. K. El-Damasy, B. Mansour, N. I. Abdel-Aziz and M. A. El-Sherbeny, Synthesis and molecular docking study of new thiazole derivatives as potential tubulin polymerization inhibitors, *ACS Omega*, 2022, **7**(37), 33599–33613.
- 19 M. S. Ebaid, H. A. A. Ibrahim, A. F. Kassem and A. Sabt, Recent studies on protein kinase signaling inhibitors based on thiazoles: review to date, *RSC Adv.*, 2024, **14**(50), 36989–37018.
- 20 S. Mishra and A. Sahu, Recent review on 1,3-thiazole derivatives as therapeutic targeted for anticancer activity, *Lett. Drug Des. Discov.*, 2024, **21**(12), 2210–2231.
- 21 S. PKN, J. Sahoo, S. K. Paidesetty and G. P. Mohanta, Thiazoles as potent anticancer agents: A review, *Indian Drugs*, 2016, **53**(11), 5–11.
- 22 R. Rana, N. Kumar, H. K. Gulati, A. Sharma, A. Khanna, R. Badhwar, *et al.*, A comprehensive review on thiazole-based conjugates as anti-cancer agents, *J. Mol. Struct.*, 2023, **1292**, 136194.
- 23 O. O. Ajani, K. T. Iyaye and O. T. Ademosun, Recent advances in chemistry and therapeutic potential of functionalized quinoline motifs – a review, *RSC Adv.*, 2022, **12**(29), 18594–18614.
- 24 O. Afzal, S. Kumar, M. R. Haider, M. R. Ali, R. Kumar, M. Jaggi and S. Bawa, A review on anticancer potential of bioactive heterocycle quinoline, *Eur. J. Med. Chem.*, 2015, **97**, 871–910.
- 25 W. S. Shehab, M. M. Amer, D. A. Elsayed, K. K. Yadav and M. H. Abdellattif, Current progress toward synthetic routes and medicinal significance of quinoline, *Med. Chem. Res.*, 2023, **32**(12), 2443–2457.
- 26 M. Ilakiyalakshmi and A. A. Napoleon, Review on recent development of quinoline for anticancer activities, *Arab. J. Chem.*, 2022, **15**(11), 104168.
- 27 S. Vandekerckhove and M. D'hooghe, Quinoline-based antimalarial hybrid compounds, *Bioorg. Med. Chem.*, 2015, **23**(16), 5098–5119.
- 28 V. Solanki, M. Ibrahim, A. Doshi, A. K. Das, H. Sarvaiya, V. Jain and Y. Jadeja, Study on synthesis, antimicrobial properties, antioxidant effects, and anticancer activity of new quinoline derivatives, *Chem. Biodivers.*, 2025, e00646.
- 29 C. Viegas-Junior, A. Danuello, V. da Silva Bolzani, E. J. Barreiro and C. A. M. Fraga, Molecular hybridization: a useful tool in the design of new drug prototypes, *Curr. Med. Chem.*, 2007, **14**(17), 1829–1852.
- 30 P. de Sena Murteira Pinheiro, L. S. Franco, T. L. Montagnoli and C. A. M. Fraga, Molecular hybridization: a powerful tool for multitarget drug discovery, *Expet Opin. Drug Discov.*, 2024, **19**(4), 451–470.
- 31 A. Erguc, M. D. Altintop, O. Atli, B. Sever, G. Iscan, G. Gormus and A. Ozdemir, Synthesis and biological evaluation of new quinoline-based thiazolyl hydrazone derivatives as potent antifungal and anticancer agents, *Lett. Drug Des. Discov.*, 2018, **15**(2), 193–202.



- 32 E. Y. Santali, Recent developments of quinoline-heterocyclic conjugates as anticancer agents, *Egypt. J. Chem.*, 2023, **66**(7), 527–551.
- 33 R. V. Patel and S. W. Park, An evolving role of piperazine moieties in drug design and discovery, *Mini Rev. Med. Chem.*, 2013, **13**(11), 1579–1601.
- 34 R. V. Patel and S. W. Park, An evolving role of piperazine moieties in drug design and discovery, *Mini Rev. Med. Chem.*, 2013, **13**(11), 1579–1601.
- 35 A. F. Brito, L. K. Moreira, R. Menegatti and E. A. Costa, Piperazine derivatives with central pharmacological activity used as therapeutic tools, *Fundam. Clin. Pharmacol.*, 2019, **33**(1), 13–24.
- 36 C. Kamili, R. S. Kakaraparthi and U. M. Vattikuti, Anti-angiogenic activity of flunarizine by in ovo, in vitro, and in vivo assays, *Turk. J. Pharm. Sci.*, 2019, **16**(3), 303.
- 37 A. K. Rathi, R. Syed, H. S. Shin and R. V. Patel, Piperazine derivatives for therapeutic use: a patent review (2010–present), *Expert Opin. Ther. Pat.*, 2016, **26**(7), 777–797.
- 38 M. T. Muhammed and E. Aki-Yalcin, Molecular docking: principles, advances, and its applications in drug discovery, *Lett. Drug Des. Discov.*, 2024, **21**(3), 480–495.
- 39 H. Komura, R. Watanabe and K. Mizuguchi, The trends and future prospective of in silico models from the viewpoint of ADME evaluation in drug discovery, *Pharmaceutics*, 2023, **15**(11), 2619.
- 40 H. Tandon, T. Chakraborty and V. Suhag, A brief review on importance of DFT in drug design, *Int. Res. J. Mod. Eng. Technol. Sci.*, 2019, **7**(4), 791–795.
- 41 H. Ciftci, M. Otsuka, M. Fujita and B. Sever, New naphthalene-linked pyrazoline-thiazole hybrids as prominent antitumor and antibreast cancer inhibitors, *Turk. J. Chem.*, 2024, **48**(6), 856–866.
- 42 M. Ferazoddin, A. B. Syeda, R. Palabindela, A. B. Syeda, G. Dasari and S. Bandari, New quinoxaline linked fused imidazo-oxazole conjugates as EGFR inhibitors: design, synthesis, in vitro anti-breast cancer evaluation, molecular docking studies and in silico ADMET, *ChemistrySelect*, 2024, **9**(48), e202403773.
- 43 R. Gavadia, J. Rasgania, N. Sahu, S. Nimesh, L. Loveleen, S. Mor, *et al.*, Indole analogs as potential anti-breast cancer agents: design, synthesis, in vitro bioevaluation with DFT, molecular docking and ADMET studies, *J. Indian Chem. Soc.*, 2024, **101**(11), 101404.
- 44 H. S. Deshmukh, V. A. Adole, U. Shah, S. N. Mali, H. Shah, R. Sarkar, *et al.*, PEG-400 mediated synthesis of benzo[d]imidazo[2,1-b]thiazoles as bioactive scaffolds: antibreast cancer potential, EGFR inhibition, antioxidant study, molecular docking, and DFT insights, *ChemistrySelect*, 2025, **10**(19), e202500521.
- 45 O. Abdulaziz, F. R. Khan, N. S. Alharthi, H. M. Alhuthali, A. Hazazi, H. A. Alzahrani, *et al.*, Computational insights into overcoming resistance mechanisms in targeted therapies for advanced breast cancer: focus on EGFR and HER2 co-inhibition, *J. Biomol. Struct. Dyn.*, 2025, **43**(8), 4215–4226.
- 46 S. Pandey, S. Mondal, K. Kajal, B. D. Kurmi, S. K. Verma and P. Patel, Current progress in the targeted therapy of breast cancer: structure–activity correlation and docking studies (2015–2021), *Arch. Pharm. (Weinheim, Ger.)*, 2023, **356**(8), 2200602.
- 47 M. Maqbool, F. Bekele and G. Fekadu, Treatment strategies against triple-negative breast cancer: an updated review, *Breast Cancer (Dove Med Press)*, 2023, 15–24.
- 48 N. T. Ueno and D. Zhang, Targeting EGFR in triple negative breast cancer, *J. Cancer*, 2011, **2**, 324.
- 49 Q. Luo, L. Zhang, Y. Hao, C. Xu, X. Wang, Z. Jia, *et al.*, Erdafitinib inhibits the tumorigenicity of MDA-MB-231 triple-negative breast cancer cells by inducing TRIM25/ubiquitin-dependent degradation of FGFR4, *Breast Cancer Res.*, 2025, **27**(1), 128.
- 50 H. M. Otfi, Targeting the inactive conformation of the epidermal growth factor receptor identifies EG31: a novel small molecule inhibitor effective against normal and 5-fluorouracil-resistant triple negative breast cancer cells, *OncoTargets Ther.*, 2025, 617–629.
- 51 J. H. Kang, N. Uddin, S. Kim, Y. Zhao, K. C. Yoo, M. J. Kim, S. A. Hong, S. Bae, J. Y. Lee, I. Shin and Y. W. Jin, Tumor-intrinsic role of ICAM-1 in driving metastatic progression of triple-negative breast cancer through direct interaction with EGFR, *Mol. Cancer*, 2024, **23**(1), 230.
- 52 N. V. Sadgir, V. A. Adole, S. L. Dhonnar and B. S. Jagdale, Synthesis and biological evaluation of coumarin appended thiazole hybrid heterocycles: Antibacterial and antifungal study, *J. Mol. Struct.*, 2023, **1293**, 136229.
- 53 O. Trott and A. J. Olson, AutoDock Vina: improving the speed and accuracy of docking with a new scoring function, efficient optimization, and multithreading, *J. Comput. Chem.*, 2010, **31**(2), 455–461.
- 54 M. B. Alhawarri, Exploring the anticancer potential of furanpydone A: A computational study on its inhibition of MTHFD2 across diverse cancer cell lines, *Cell Biochem. Biophys.*, 2025, **83**(1), 437–454.
- 55 M. N. Ahmadabadi, E. Rezaee, M. Nematpour, L. Karami, S. Mokhtari, F. Kobarfard and S. A. Tabatabai, Synthesis, molecular dynamics simulation, and in-vitro antitumor activity of quinazoline-2,4,6-triamine derivatives as novel EGFR tyrosine kinase inhibitors, *Iran. J. Pharm. Res.*, 2023, **21**(1), e133840.
- 56 A. Daina, O. Michielin and V. Zoete, SwissADME: a free web tool to evaluate pharmacokinetics, drug-likeness and medicinal chemistry friendliness of small molecules, *Sci. Rep.*, 2017, **7**, 42717.
- 57 V. A. Adole, A. Kumar, N. Misra, R. A. Shinde and B. S. Jagdale, Synthesis, computational, antimicrobial, antioxidant, and ADME study of 2-(3,4-dimethoxyphenyl)-4H-chromen-4-one, *Polycycl. Aromat. Compd.*, 2023, **43**(1), 1–15.
- 58 K. B. Gangurde, V. A. Adole and D. S. Ghotekar, Computational study: synthesis, spectroscopic (UV-vis, IR, NMR), antibacterial, antifungal, antioxidant, molecular docking and ADME of new (E)-5-(1-(2-(4-(2,4-



- dichlorophenyl)thiazol-2-yl)hydrazineylidene)ethyl)-2,4-dimethylthiazole, *Results Chem.*, 2023, **6**, 101093.
- 59 V. A. Adole, Computational approach for the investigation of structural, electronic, chemical and quantum chemical facets of twelve Biginelli adducts, *Organomet. Chem.*, 2021, **1**(1), 29–40.
- 60 M. J. Frisch, G. W. Trucks, H. B. Schlegel, G. E. Scuseria, M. A. Robb, J. R. Cheeseman, V. G. Zakrzewski, J. A. Montgomery, T. Vreven, K. N. Kudin and J. C. Burant, *Gaussian 03, Revision C.02. Wallingford (CT)*, Gaussian Inc., 2004.
- 61 A. D. Becke, Density-functional thermochemistry. III. The role of exact exchange, *J. Chem. Phys.*, 1993, **98**(7), 5648–5652.
- 62 C. Lee, W. Yang and R. G. Parr, Development of the Colle–Salvetti correlation-energy formula into a functional of the electron density, *Phys. Rev. B*, 1988, **37**(2), 785–789.
- 63 R. D. I. I. Dennington, T. Keith and J. Millam, *GaussView, Version 4.1.2. Shawnee Mission (KS)*, Semichem Inc., 2007.

